We are IntechOpen, the world's leading publisher of Open Access books Built by scientists, for scientists

6,900
Open access books available

185,000
International authors and editors

200M
Downloads

Our authors are among the

154
Countries delivered to

TOP 1%
most cited scientists

12.2%
Contributors from top 500 universities

WEB OF SCIENCE™

Selection of our books indexed in the Book Citation Index in Web of Science™ Core Collection (BKCI)

Interested in publishing with us?
Contact book.department@intechopen.com

Numbers displayed above are based on latest data collected.
For more information visit www.intechopen.com

Chapter

Electro-Optical Manipulation Based on Dielectric Nanoparticles

Jiahao Yan and Yuchao Li

Abstract

The ability to dynamically modulate plasmon resonances or Mie resonances is crucial for practical application. Electrical tuning as one of the most efficiently active tuning methods has high switching speed and large modulation depth. Silicon as a typical high refractive index dielectric material can generate strong Mie resonances, which have shown comparable performances with plasmonic nanostructures in spectral tailoring and phase modulation. However, it is still unclear whether the optical response of single silicon nanoantenna can be electrically controlled effectively. In this chapter, we introduce two types of optoelectronic devices based on Mie resonances in silicon nanoantennas. First, we observe obvious blueshift and intensity attenuation of the plasmon-dielectric hybrid resonant peaks when applying bias voltages. Second, photoluminescence (PL) enhancement and modulation are achieved together in the WS_2-Mie resonator hybrid system.

Keywords: silicon nanoparticles, silicon nanostripes, WS_2, active control, photoluminescence manipulation

1. Introduction

Dynamically controlling the optical responses from plasmonic or Mie resonators is significant for future optical signal processing [1, 2]. Among different active tuning methods, electrical tuning is one of the most effective one owing to high switching speed and large tuning ranges [3–5]. Recently, electrical tuning on metamaterials based on plasmonic nanostructures has been reported, and the control mechanisms rely on semiconductor layers [6–8], graphene [9–13], or electromechanical deformation [14, 15]. Nevertheless, there are few works about the optoelectronic modulation on nanoscale devices up to now. Furthermore, how to realize the electrical tuning on single nanoparticles is still a challenge.

Combining optical nanoantennas with atomically thin WS_2 may be another method to realize dynamic optical responses. Atomically thin WS_2 (monolayer or bilayer) exhibits intriguing electrical and optical properties [16–18]. Monolayer WS_2 shows strong excitonic emission peak at visible wavelengths; however, ultrathin thickness hinders further enhancement of excitonic emission. Near-field enhancements at excitation wavelengths can enhance the light absorbance, while that at emission wavelengths would boost the emission rate, so those two factors both enhance the excitonic emission from WS_2. Based on it, many efforts have been made to realize field enhancements via plasmonic nanostructures and photonic crystals at both excitation and emission wavelengths.

Silicon nanoantennas as a typical dielectric Mie resonator have wide application prospect in building metasurfaces [19–21], nonlinear optics [22], and biosensing [23]. They may be better choice than plasmonic structures and photonic crystals in building electrically controlled devices. The Mie resonances in silicon nanoantennas can be modulated through changing the sizes [24, 25] or crystallographic phases [20] passively. However, how to realize active control based on the Mie resonances in silicon nanocavities is still a challenge. Besides changing the optical properties of Mie resonators intrinsically, active tuning may also be realized via coupling with 2D materials. Neshev et al. have theoretically demonstrated the PL modulation of 2D materials based on the directional emission caused by Mie resonators [26]. Recently, the first experimental work has been done, in which a forward-to-backward emission ratio of 20 was realized because of the interaction between MoS_2 monolayer and Mie resonators [27]. However, both of them were analyzed on passive control.

2. Electrically controlled optical responses of silicon-based nanoantennas

In this chapter, we will discuss the applications of silicon-based Mie resonators into electro-optical modulation. This chapter can be divided into two parts:

First, we demonstrated the electrically tunable scattering of a single silicon nanoparticle at visible wavelengths. To build the nanoantennas, gold interdigital electrodes with separation distances between 100 and 200 nm were fabricated using photolithography and focused ion beam (FIB) milling. After trapping silicon nanoparticles with different sizes between adjacent two electrodes, the scattering spectra under different voltages can be measured. Interestingly, the scattering experiences blueshift and obvious intensity attenuation when increasing the applied voltages from 0 to 1.5 V. In theory, MIS (metal-insulator-semiconductor) junctions can be formed at Au-SiO_2-Si interfaces [28]. Once the bias voltage increases, the inversion and accumulation effect would produce much more free carriers at interfaces [29–31] and then change the permittivity based on Drude model [32, 33]. The proposed hybrid nanoantennas represent a new method to build optoelectronic devices based on Mie resonators.

Second, we combined silicon nanostripes, a typical Mie resonator, with WS_2 to realize active PL manipulation. In the proposed electro-optical modulator, suspended monolayer and bilayer WS_2 are covered on a Si nanostripe. The Si nanostripe not only acts as a nanoscale gate electrode but also a Mie resonator. For both monolayer and bilayer WS_2, the PL intensities on the nanostripes are much stronger than those of the suspended one. After applying gate voltages, both the electrostatic doping and strain come into effect. This new tuning mechanism leads to abnormal control of exciton emission from WS_2, which is clearly different from that in previous works [34–36]. Considerable PL tuning can also be observed in bilayer WS_2 gated by Si nanostripes. Based on the modulation capability, we believe the proposed electro-optical modulator will bring new possibilities for future nanophotonic devices.

3. Hybrid nanoantennas based on silicon nanoparticles and nanostripes

3.1 Electrically driven scattering in a hybrid dielectric-plasmonic nanoantenna

In order to build an electrically controlled silicon nanoantenna, the biggest issue is how to apply voltage on a single nanoparticle and collect the electrically

modulated signals with low noise. The design of electrically tunable silicon nanoantenna is shown in **Figure 1a**. First, maskless laser lithography and electron-beam deposition were used to fabricate Au electrodes with the thickness of 100 nm on the Si/SiO_2 substrate, and the thickness of SiO_2 layer is 300 nm. In our design, several large Au electrodes (200 × 400 μm) are deposited with a row of holes in the center. Second, the connected area in the center was nano-patterned using FIB milling to form nanoscale interdigital electrode structure. The separation distance between adjacent nano-electrodes is adjusted from 100 to 200 nm to match the size distributions of silicon nanoparticles, since the silicon nanoparticles fabricated through femtosecond laser ablation in liquid (fs-LAL) have a wide size distribution. Finally, during the evaporation process, the silicon nanoparticles in colloid have a certain probability to be trapped in the gaps.

Before studying the optical properties of Si-Au hybrid nanoantennas, we should study the Au electrode platform first. For the fabricated Au grating, due to the incident light that comes from a dark-field circle in the objective, wave vectors with different directions at x-y plane cannot launch surface plasmon polariton efficiently. In addition, the plasmon energy mainly decays nonradiatively through near-field coupling between adjacent Au electrodes, so Au gratings cannot show bright scattering as shown in **Figure 1b**. However, if only two electrodes left (see **Figure 1b**), localized surface plasmon can be formed between two Au electrodes. Strong scattering light can be generated from the plasmonic field enhancement in the gap. Therefore, we use Au grating in experiment whose scattering can be ignored compared with Si nanoparticles. Typical Au electrode-loaded Si nanoparticles are shown in **Figure 1c** and **d**, where a bright dot can be seen in dark-field image which means the scattering from the Si nanoantenna. In spectral measurement, through moving the scattering spot into the center of slit and only extracting the data from the location of nanoparticle, the exact scattering from the Si nanoparticle can be obtained.

For isolated Si nanoparticles, the resonant modes depend on particle sizes and particle numbers according to Mie theory. While for Au electrode-loaded Si

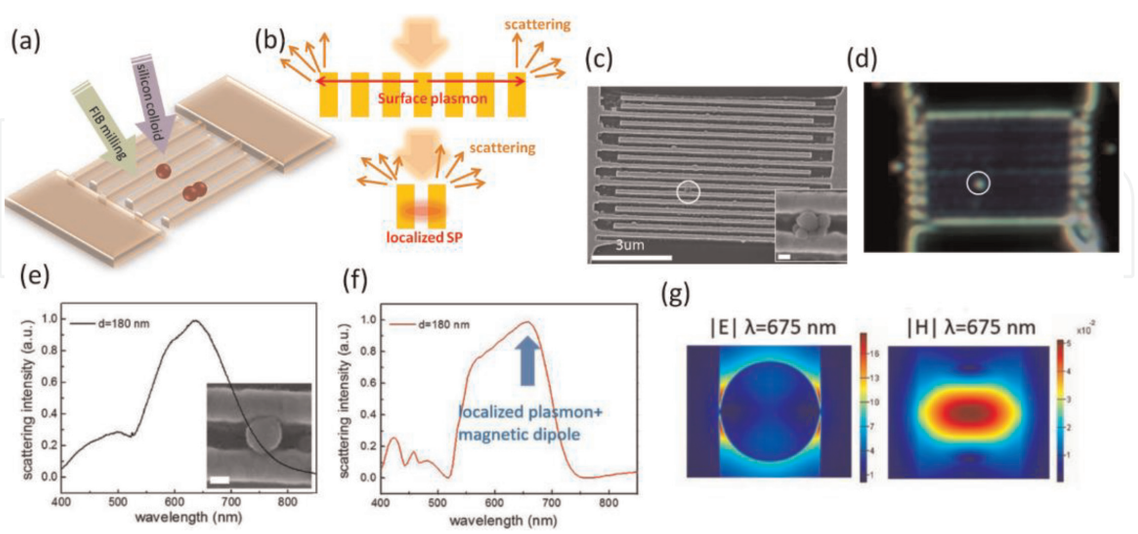

Figure 1.
Optical properties of the silicon nanoantenna. (a) A schematic diagram explains the fabrication of Au electrode-loaded Si nanoparticles. (b) The schematic shows different plasmon resonant modes of two types Au electrodes. (c) The scanning electron microscope (SEM) image of Au interdigital electrodes with a silicon NP trapped among them. Inset is the high magnification SEM image with a scale bar of 100 nm. (d) The dark-field scattering image of the sample in (c). The white circle reveals the location of Si nanoparticles. (e, f) Measured scattering spectrum of a 180 nm Si nanoparticle (e) and the corresponding simulated scattering spectrum (f). (g) The electric and magnetic field distributions at 675 nm, which represent the hybrid modes coupling between localized plasmon and magnetic dipole.

nanoparticles, the mode coupling between nanoparticles and Au electrodes also needs to be considered. The hybrid nanoantennas may exhibit different scattering spectra at visible wavelengths. Therefore, it is necessary to study the scattering spectra without applied voltage first. Although self-assembled process is random, desirable and representative nanoparticles can be found through matching and positioning. **Figure 1e** shows 180 nm Si nanoparticles between two Au electrodes with a spacing slightly less than 180 nm. The measured scattering spectra exhibits a single broad peak around $\lambda = 650\,nm$. As shown in **Figure 1f**, the simulated spectrum is very similar to experimental spectrum. Corresponding electric and magnetic field distributions in **Figure 1g** demonstrate the existence of circular magnetic field distributions and strong electric field enhancement at interfaces, which means the scattering peak is generated from the interaction between the Mie-type magnetic dipole mode in Si nanoparticles and the localized surface plasmon resonances (LSPR) at Au-Si interfaces.

The electrical properties of the Si-Au hybrid devices were measured using a semiconductor parameter analyzer. The measured I-V curve is shown in **Figure 2a**, and we can conclude that the Si-Au interfaces can be regarded as Schottky junctions. From 0 to 1.5 V, the current increases nonlinearly with the voltage. For the fabricated Si nanoparticles, thin oxide (1–2 nm) shells will be formed inevitably in the air. Therefore, the interfaces are MIS junctions whose current is generated through tunnel effect and plasmon hot electron injection. For MIS junctions, the band bends upward at interfaces when no voltage applies as the schematic diagram shown in **Figure 2b**. Depletion region forms at the interfaces and free carriers move away from interfaces based on the band bending [29]. With applied bias, surface potential at two interfaces increases. The carrier concentration at the MIS junction under lower potential was greatly increased because the downward energy band realizes the accumulation of electrons. The other MIS junction under higher potential could form an inversion layer if the applied voltage is high enough. When the intrinsic energy level crosses the Fermi level [29–31], the hole density would greatly increase under the inversion state. The charge densities at surface at different applied voltages can be estimated by the following equations [29]

$$|Q_{inv}| = -C_{ox}(V_G - V_T) \propto \exp\left(\frac{\beta\Psi_S}{2}\right) \tag{1}$$

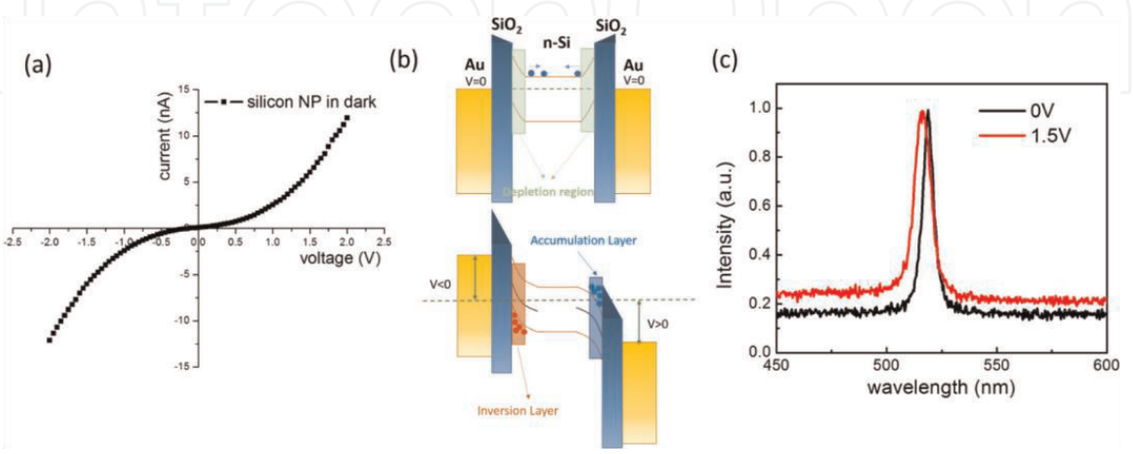

Figure 2.
Analysis on the voltage-induced carrier injection. (a) The I-V curve of a fabricated Si-Au hybrid structure. (b) Schemes for the band bending and carrier distribution with and without applied voltage. (c) The Raman spectrum of a loaded nanoparticle before and after applied voltage (1.5 V).

$$|Q_{acc}| = C_{ox}(V_G - V_{FB}) \propto \exp\left(\frac{-\beta\Psi_S}{2}\right) \tag{2}$$

where Q_{acc} and Q_{inv} are the carrier densities at accumulation and inversion regions. C_{ox} is the capacitance of thin insulator layer. V_G is the applied bias. V_{FB} and V_T are accumulation and inversion effects related to voltages. $\beta = q/k_BT$ is a constant. Ψ_S is the surface potential at interfaces. Based on the electric field we applied and above calculation, the electron or hole concentrations can be increased by more than three orders of magnitude in accumulation or inversion regions, respectively [29]. The Raman signals under different voltages are presented in **Figure 2c**. With 1.5 V applied bias, the resonant peak of silicon just red shifts slightly, and this weak shift means the temperature variation is less than 100 K [37]. Therefore, we can exclude the influence of thermal effect on the refractive index since the refractive index of silicon only increases 3.85×10^{-4} per degree [38].

To examine whether the mechanism discussed above could affect the optical properties significantly, the scattering spectra of the typical silicon nanoantenna with applied bias were presented in **Figure 3a**. To ensure stability, all scattering data were collected in 1 min during the increase of voltage from 0 to 1.5 V. Because the interfaces of the fabricated hybrid nanoantenna are symmetric, we only need to collect the scattering spectra under forward bias which is enough to embody the properties of hybrid nanoantennas. For a typical hybrid nanoantenna as shown in **Figure 3a** with a 180 nm Si nanoparticle, we can observe the suppression of hybrid plasmon-Mie resonant peaks when increasing the voltages. The magnetic dipole peak was dominated when no voltage applies. However, when applied voltage reaches 1.5 V, the electric dipole peak at shorter wavelength becomes the more prominent one.

As discussed above, different applied voltages result in different free carrier concentrations of Si nanoparticles. Further, we should clarify how carrier injection influences the dielectric function of silicon. The modulation mechanism is based on free carrier-induced refractive index change. Although electric field cannot change the refractive index of bulk silicon or whole silicon nanostructures significantly as previous works reported [39], obvious refractive index modification can be realized at accumulation and inversion interfaces. From the field profiles, one can understand the refractive index change on surface is enough to change optical responses because field enhancements and radiative decays mainly come from interfaces. How free carriers contribute to the refractive index change at interfaces can be described by the Drude model

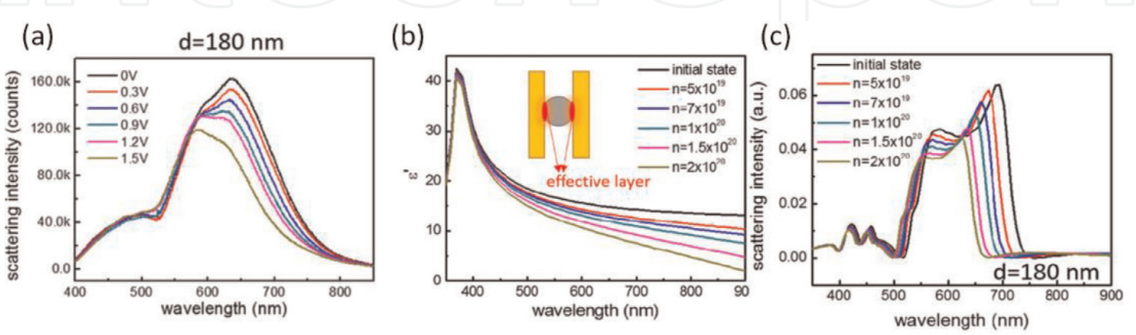

Figure 3.
Electrically controlled scattering. (a) Scattering spectra of the 180 nm Si nanoparticles when applied voltages equal to 0, 0.3, 0.6, 0.9, 1.2, and 1.5 V. (b) The variation trend of the real part of permittivity at Au-SiO_2-Si interfaces when increasing the carrier concentrations. (c) The calculated scattering spectra of the 180 nm Si nanoparticle under different carrier concentrations at interfaces.

$$\Delta\varepsilon' = -\frac{\varepsilon_\infty \omega_p^2 \tau^2}{1+\omega^2\tau^2} \tag{3}$$

$$\Delta\varepsilon'' = \frac{\varepsilon_\infty \omega_p^2 \tau}{\omega(1+\omega^2\tau^2)} \tag{4}$$

where ω_p is the plasma frequency which is defined as $\omega_p = \sqrt{Ne^2/m_C\varepsilon_\infty\varepsilon_0}$. τ is the damping time equals to $\mu m_C/e$ where e is the charge of an electron. m_C is the effective mass, ε_0 is the vacuum permittivity, and ε_∞ is the permittivity of silicon at visible band. N is the concentration of free carrier which determines the changes of permittivity. Using the Drude model discussed above, we can calculate how free carriers influence the dielectric function of silicon as shown in **Figure 3b**. Putting different carrier concentrations (10^{17} to $2.0 \times 10^{20}\,\mathrm{cm}^{-3}$) into Drude model, one can see the real part of permittivity decreases gradually especially at longer wavelengths from 600 to 900 nm. Because the accumulation and inversion layers are less than 5 nm at interfaces, we only used the free carrier-induced dielectric functions at interfaces for the numerical simulation. As shown in **Figure 3c**, the simulated scattering spectra under different carrier concentrations are very similar to the corresponding measured spectra under different applied bias. For the 180 nm Si nanoparticle (see **Figure 3c**), the hybrid resonant peak experiences blueshift and intensity attenuation when increasing the carrier concentrations in sequence. The attenuation trend of resonant peaks is very similar to the experimental spectra in **Figure 3a**. Our proposed structures provide an opportunity to collect the electrically controlled scattering signals on single-particle level.

3.2 PL enhancements enabled by silicon nanostripes

Owing to the unique properties of dielectric Mie resonators, researchers are trying to use Mie resonators as an important building block to form new-generation electro-optical modulators. One strategy is to combine Mie resonators with 2D materials as the schematic shown in **Figure 4a**. WS_2 monolayers and bilayers were obtained by mechanical exfoliation and all-dry transfer technique. WS_2 layers and Si nanostripes were aligned and contacted under an optical microscope. Si nanostripes were fabricated by FIB milling onto SiO_2 coated silicon-on-insulator (SOI) wafers. Gold electrodes were patterned and deposited on WS_2 and bare silicon to build source, drain, and gate. A simple cross-section schematic of the substrate in **Figure 4a** shows that there is an insulator layer between the Si substrate and the top Si film. Therefore, the scattering from Si nanostripes is not only pure Mie effect but the Mie resonance combined with the Fabry-Perot effect. In our case, the thickness of the insulator layer (h) is 375 nm. The dark-field scattering spectrum and the corresponding optical image in **Figure 1b** indicate that Si nanostripes have a broadband resonant peak. Dominant peaks are located around 700 nm, and two small peaks can also be distinguished below $\lambda = 600\,\mathrm{nm}$. **Figure 4c** is a typical WS_2-Si nanostripe hybrid nanostructure. Corresponding SEM images are shown in **Figure 4d**. From SEM images, we can see the width of Si nanostripe is around 650 nm surrounded by two $10 \times 30\,\mu m$ etched regions. Wrinkles and missing regions are inevitably formed during the transfer and lift-off processes. Fortunately, these regions can be avoided in the following measurements.

Figure 5a indicates different locations we measured on bilayer and monolayer WS_2. From the PL emission spectra of monolayer WS_2 as shown in **Figure 5b**, one can conclude Si nanostripes can increase the PL intensities but less than threefold compared with that in the suspended region. It should be noticed that the

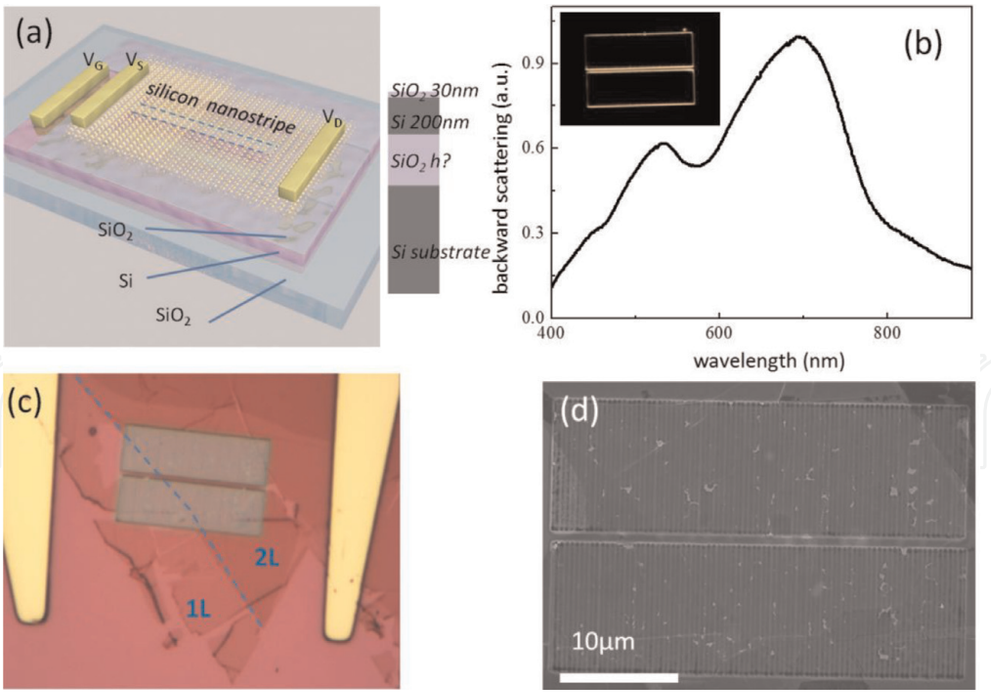

Figure 4.
Experimental design for the WS_2-Si nanostripe hybrid structure. (a) Schematic illustration of the electrically controlled device and the cross section of the SiO_2-coated SOI substrate. (b) Dark-field backward scattering of the fabricated Si nanostripe. Inset: The dark-field optical image. (c) The bright-field optical image of a typical device. Monolayer and bilayer regions are labeled as 1L and 2L. (d) The corresponding SEM image.

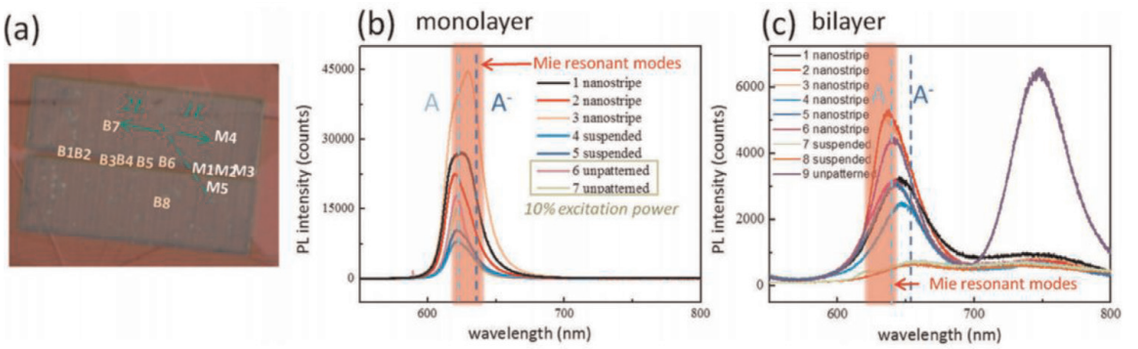

Figure 5.
PL enhancements in monolayer and bilayer WS_2. (a) The optical image showing the detection points on monolayer (M) and bilayer (B) WS_2. (b, c) PL spectra of different positions marked in (a). The locations of exciton (A) and trion (A^-) states are labeled, along with the range of Mie resonant modes (marked by red stripe).

unpatterned region can also enhance the PL intensity and the enhancement performance is better than that on the Si nanostripe. For bilayer WS_2, the PL enhancement is much more significant as shown in **Figure 5c**. The bilayer WS_2 on the Si nanostripe possesses nearly 10 times larger PL intensities than the suspended area. Interestingly, this PL enhancement was only observed at $\lambda = 625$ nm where direct bandgap transition happens. However, for unpatterned area, PL intensities at both direct and indirect transition wavelengths ($\lambda = 635\&750$ nm) are enhanced. The performances of PL enhancement for direct transition are comparable for unpatterned area and the Si nanostripe. Moreover, unpatterned area can strengthen the indirect transition more than 10 times. Besides the differences of PL intensities, the line shapes also change in **Figure 5b** and **c** which reveals the conversion between exciton (A) and trion (A^-). The locations of exciton and trion emission are labeled in **Figure 5b** and **c**. Further peak fitting demonstrates the decreased trend of trion emission from suspended area and nanostripes to the unpatterned region. Substrate

effect and the optical resonant modes may be two reasons that lead to the change of line shapes. The Fabry-Perot mode in the unpatterned substrate and Fabry-Perot mode assisted by Mie resonances in fabricated nanostripes can both influence the PL line shapes.

3.3 PL manipulation of monolayer and bilayer WS_2 gated by silicon nanostripes

Realizing the electrical tuning is crucial for further application. To examine the electrical tuning performance, first, PL intensities of monolayer WS_2 under different voltages were measured as shown in **Figure 6a**. When applying negative gate voltages from 0 to −10 V, the maximum PL intensity increases by 50%. On the contrary, the intensity of the PL peak decreases to half under positive gate voltages from 0 to 10 V. Compared with the normal WS_2 monolayer gated by the flat gate [34–36], the PL enhancement effect is weaker, while the reduction effect is more obvious. This phenomenon indicates that the tuning effect is not pure electrostatic doping and there should be a new mechanism. PL changes of the bilayer WS_2 under different voltages were also measured as shown in **Figure 6b** and **c**. Unexpectedly, the variation trends under positive and negative gate voltages are almost the same. The maximum PL intensity doubled when increasing the gate voltage from 0 to 10 V. Several groups have studied the electrically controlled PL of bilayer WS_2, while no obvious effect has been observed [34–36]. Therefore, the obvious PL enhancement we observed may not arise from pure electrostatic doping. The gate voltage dependent intensity of excitonic peak is plotted in **Figure 6d**. The PL intensity of monolayer WS_2 increases linearly with gate voltage, while the PL intensity of bilayer WS_2 and the gate voltage follow a parabolic relationship.

How to explain the abnormal PL manipulation in the proposed hybrid nanoantennas? The schematic shown in **Figure 7a** may give a better understanding.

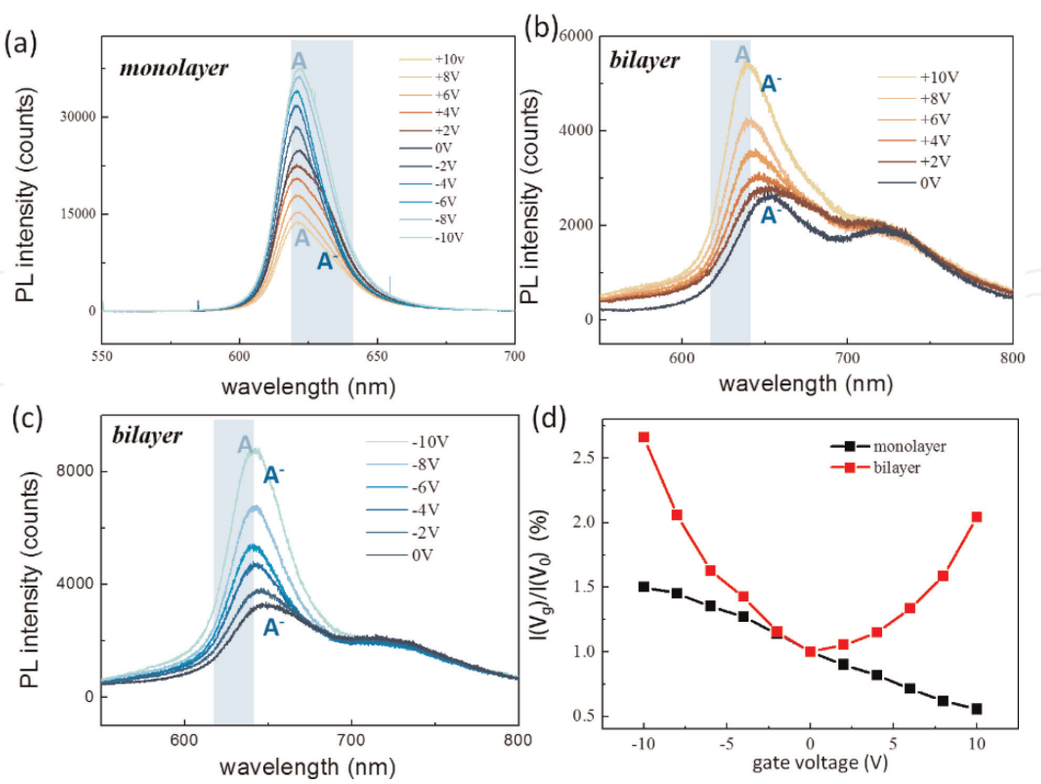

Figure 6.
Electrically controlled PL. (a) PL spectra of the monolayer WS_2 on the Si nanostripe at different gate voltages. (b, c) PL spectra of the bilayer WS_2 on the Si nanostripe at different gate voltages. (d) The gate voltage dependence of PL intensities.

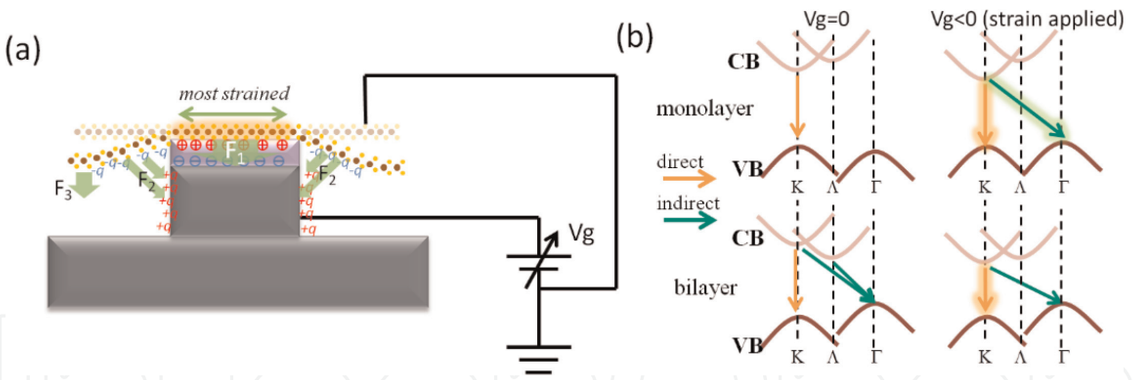

Figure 7.
Mechanism of electrical tuning. (a) Schematic setup showing how tensile strain can be generated by electrostatic gating. F_1, F_2, and F_3 represent three types of electrostatic forces. (b) Schematic diagram showing the changes of band structure and dominated transitions before and after applying strain.

When placing WS_2 flakes on the Si nanostripe, there are three regions that experience different forces. The first part is WS_2 on the Si nanostripe, the second part is WS_2 near the edges of Si nanostripes, and the third part is fully suspended WS_2. If the applied voltage is high enough, a great number of holes and electrons will be produced at WS_2 layers and bottom Si nanostructures, respectively. Besides the electrostatic doping, the static electric field can also produce attractive forces. As shown in **Figure 7a**, there are three types of attractive forces F_1, F_2, and F_3 which depend on different distances and capacitances. F_1 is the attractive force between adherent WS_2 and Si nanostripe through the 30 nm insulator layer. F_2 is the attractive force between suspended WS_2 around edges and the Si nanostripe. F_2 at edges equals to F_1 and decreases gradually away from the Si nanostripe, so this force will let WS_2 at edges be curved and exert a large uniaxial tensile strain on WS_2. The electrostatic attraction between the suspended WS_2 and bottom Si (F_3) is much weaker which can be ignored because of a larger distance and smaller capacitance. The deflection of few layer WS_2 Δl under electrostatic force can be calculated by equation [40]:

$$PL^2 = 8T_0 t\Delta l + \frac{64}{3}\frac{Et}{L^2(1-\upsilon^2)}\Delta l^3 \tag{5}$$

where t is the thickness that equals to 0.8 or 1.6 nm, E is the Young's modulus of WS_2, and L is the effective length of strained WS_2. The effective length is very small because only WS_2 at edges experiences significant attractive forces. $P = {(C^2V_g^2)}/{2\varepsilon_0}$ is the electrostatic pressure, where C is the capacitance per unit area and ε_0 is the permittivity of vacuum. After considering the relationship between strain and the deflection, the strain can be estimated by [40]:

$$\chi = 2\Delta l^2/L^2 = 2[(3/64)(PL)/(Et)]^{2/3} \tag{6}$$

Based on the calculation above, the strain χ within effective area is larger than 2.8%. Such high strain is able to change the band structure of WS_2 and influence the excitonic emission [41–43]. Therefore, in **Figure 7b**, we combine electrostatic doping and strain effect together to analyze the change of band structure and PL intensity. For 1L-WS_2, if only electrostatic doping comes into effect, negative gating would enhance the PL intensity contributed by direct transition. However, in our case, larger strain generated from attractive forces changes the band gap of monolayer WS_2. Without applied bias, the locations of valence-band maximum and conduction-band minimum are overlapped at the point K. Once strain is applied,

the valence-band maximum will shift from K to Γ point, and indirect transition will happen. Therefore, the strain effect will weaken the PL intensity, which has opposite effect compared with electrostatic doping under negative gating. As a consequence, the PL enhancement is weaker under negative gating and more obvious under positive gating compared with previous works. For 2L-WS_2, electrostatic effect can be ignored, and the strain effect is dominated. Without applied bias, the PL emission of bilayer WS_2 contains both direct transitions and indirect transitions. If the strain becomes larger, valence-band maximum at the K point reduces, which promotes the direct transition along the K − K direction [43, 44].

4. Dielectric nanoparticles for bionanosensing

From the above analysis, we know that Mie resonators such as Si nanoparticles can combine with plasmonic nano-electrodes to obtain electrically controlled optical responses, and Mie resonators such as Si nanostripes can also interact with WS_2 layers to realize abnormal electro-optical modulation based on electrostatic doping and strain effect. Further, it is necessary to utilize the unique properties of Mie resonators and analyze their application prospect in biosensing.

As we know, plasmonic nanostructures have been widely used in biosensing. Plasmon resonances experience redshift when increasing the surrounding refractive index, which is the most basic mechanism of biosensing. Dielectric Mie resonators have low-loss feature and strong directional scattering which also have a potential as biosensing nanoantennas. However, based on current reports and our experiments, we found the optical responses of single silicon nanostructures such as Si nanoparticles cannot exhibit obvious change when changing the surrounding refractive index. Therefore, the biosensor based on a single Si nanoparticle is insensitive.

Fortunately, we found the scattering spectra become very sensitive to surrounding refractive index if single Si nanoparticles combine to dimers or other oligomers. Based on our theoretical analysis, touching Si nanoparticles can produce strong electric field enhancement in the gap. This gap electric mode is a key factor for sensitive spectral change, because the gap electric mode would enhance and experience redshift with the increase of surrounding refractive index. As talked above, 1–2 nm silica layer is naturally grown on Si nanoparticles. Based on the mature biomarker technique, we can easily modify the silica surface with specific functional groups and realize the detection of many kinds of biomolecules. Furtherly, Si nanoparticles can be injected into living cells to realize the sensing in vivo. Finally, we can combine the biosensing and optoelectronic property of Mie resonators to build new type biosensors. On the one hand, biomolecules can change the electrical properties of dielectric nanostructures and then influence the optical signals. On the other hand, biomolecules can change the optical properties of nanoantennas and furtherly influence the electrical readout.

5. Conclusions

In this chapter, we have introduced the electrically controlled scattering of individual Mie resonators and PL from the WS_2-Mie resonator hybrid system. The strong magnetic responses and low-loss feature make silicon-based Mie resonators become important building blocks in nanophotonics. Combining top-down and bottom-up fabrication methods, plasmon-Mie hybrid nanostructures and WS_2-Mie hybrid nanostructures are fabricated, respectively. These structures give us an

opportunity to apply voltages at nanoscale and collect the optical signals at single points. Interfaces are important in those hybrid nanodevices. The interfaces between plasmonic structures and Mie resonators bring new mechanism on carrier injection and changes of refractive index, while the contact between WS_2 and Mie resonator generates unique PL active tuning arising from the synergistic effect between electrical doping and tensile strain under gate voltages. In the emerging applications based on dielectric Mie resonators, our findings provide an important and feasible method to build optoelectronic functional devices that can transfer electrical signal to optical signal. Furthermore, the excellent biosensing performance will expand the applications of Mie resonator-based optoelectronic devices.

Acknowledgements

This work was supported by the National Natural Science Foundation of China (No. 11774135, 11874183, and 61827822).

Conflict of interest

The authors declare no competing financial interests.

Author details

Jiahao Yan and Yuchao Li*
Institute of Nanophotonics, Jinan University, Guangzhou, China

*Address all correspondence to: liyuchao@jnu.edu.cn

IntechOpen

© 2019 The Author(s). Licensee IntechOpen. This chapter is distributed under the terms of the Creative Commons Attribution License (http://creativecommons.org/licenses/by/3.0), which permits unrestricted use, distribution, and reproduction in any medium, provided the original work is properly cited.

References

[1] Lee SH, Choi M, Kim T-T, Lee S, Liu M, Yin X, et al. Switching terahertz waves with gate-controlled active graphene metamaterials. Nature Materials. 2012;**11**:936-941. DOI: 10.1038/nmat3433

[2] Kang L, Lan S, Cui Y, Rodrigues SP, Liu Y, Werner DH, et al. An active metamaterial platform for chiral responsive optoelectronics. Advanced Materials. 2015;**27**:4377-4383. DOI: 10.1002/adma.201501930

[3] Kern J, Kullock R, Prangsma J, Emmerling M, Kamp M, Hecht B. Electrically driven optical antennas. Nature Photonics. 2015;**9**:582-586. DOI: 10.1038/nphoton.2015.141

[4] Fan P, Yu Z, Fan S, Brongersma ML. Optical Fano resonance of an individual semiconductor nanostructure. Nature Materials. 2014;**13**:471-475. DOI: 10.1038/nmat3927

[5] Prangsma JC, Kern J, Knapp AG, Grossmann S, Emmerling M, Kamp M, et al. Electrically connected resonant optical antennas. Nano Letters. 2012;**12**:3915-3919. DOI: 10.1021/nl3007374

[6] Chen H-T, Padilla WJ, Zide JM, Gossard AC, Taylor AJ, Averitt RD. Active terahertz metamaterial devices. Nature. 2006;**444**:597-600. DOI: 10.1038/nature05343

[7] Chen H-T, Lu H, Azad AK, Averitt RD, Gossard AC, Trugman SA, et al. Electronic control of extraordinary terahertz transmission through subwavelength metal hole arrays. Optics Express. 2008;**16**:7641-7648. DOI: 10.1364/OE.16.007641

[8] Jun YC, Gonzales E, Reno JL, Shaner EA, Gabbay A, Brener I. Active tuning of mid-infrared metamaterials by electrical control of carrier densities. Optics Express. 2012;**20**:1903-1911. DOI: 10.1364/OE.20.001903

[9] Mousavi SH, Kholmanov I, Alici KB, Purtseladze D, Arju N, Tatar K, et al. Inductive tuning of Fano-resonant metasurfaces using plasmonic response of graphene in the mid-infrared. Nano Letters. 2013;**13**:1111-1117. DOI: 10.1021/nl304476b

[10] Emani NK, Chung T-F, Kildishev AV, Shalaev VM, Chen YP, Boltasseva A. Electrical modulation of fano resonance in plasmonic nanostructures using graphene. Nano Letters. 2013;**14**:78-82. DOI: 10.1021/nl403253c

[11] Yao Y, Shankar R, Kats MA, Song Y, Kong J, Loncar M, et al. Electrically tunable metasurface perfect absorbers for ultrathin mid-infrared optical modulators. Nano Letters. 2014;**14**: 6526-6532. DOI: 10.1021/nl503104n

[12] Yao Y, Kats MA, Genevet P, Yu N, Song Y, Kong J, et al. Broad electrical tuning of graphene-loaded plasmonic antennas. Nano Letters. 2013;**13**: 1257-1264. DOI: 10.1021/nl3047943

[13] Valmorra F, Scalari G, Maissen C, Fu W, Schönenberger C, Choi JW, et al. Low-bias active control of terahertz waves by coupling large-area CVD graphene to a terahertz metamaterial. Nano Letters. 2013;**13**:3193-3198. DOI: 10.1021/nl4012547

[14] Ou J-Y, Plum E, Zhang J, Zheludev NI. An electromechanically reconfigurable plasmonic metamaterial operating in the near-infrared. Nature Nanotechnology. 2013;**8**:252-255. DOI: 10.1038/nnano.2013.25

[15] Chen K, Razinskas G, Feichtner T, Grossmann S, Christiansen S, Hecht B. Electromechanically tunable suspended optical nanoantenna. Nano Letters.

2016;**16**:2680-2685. DOI: 10.1021/acs.nanolett.6b00323

[16] Wang QH, Kalantar-Zadeh K, Kis A, Coleman JN, Strano MS. Electronics and optoelectronics of two-dimensional transition metal dichalcogenides. Nature Nanotechnology. 2012;**7**:699-712. DOI: 10.1038/nnano.2012.193

[17] Zhao W, Ghorannevis Z, Chu L, Toh M, Kloc C, Tan P-H, et al. Evolution of electronic structure in atomically thin sheets of WS_2 and WSe_2. ACS Nano. 2012;**7**:791-797. DOI: 10.1021/nn305275h

[18] Fiori G, Bonaccorso F, Iannaccone G, Palacios T, Neumaier D, Seabaugh A, et al. Electronics based on two-dimensional materials. Nature Nanotechnology. 2014;**9**:768-779. DOI: 10.1038/nnano.2014.207

[19] Li Y, Kita S, Muñoz P, Reshef O, Vulis DI, Yin M, et al. On-chip zero-index metamaterials. Nature Photonics. 2015;**9**:738-742. DOI: 10.1038/nphoton.2015.198

[20] Zywietz U, Evlyukhin AB, Reinhardt C, Chichkov BN. Laser printing of silicon nanoparticles with resonant optical electric and magnetic responses. Nature Communications. 2014;**5**:3402. DOI: 10.1038/ncomms4402

[21] Arbabi A, Horie Y, Bagheri M, Faraon A. Dielectric metasurfaces for complete control of phase and polarization with subwavelength spatial resolution and high transmission. Nature Nanotechnology. 2015;**10**:937-943. DOI: 10.1038/nnano.2015.186

[22] Ma C, Yan J, Liu P, Wei Y, Yang G. Second harmonic generation from an individual all-dielectric nanoparticle: Resonance enhancement versus particle geometry. Journal of Materials Chemistry C. 2016;**4**:6063-6069. DOI: 10.1039/C6TC01635A

[23] Yan J, Liu P, Lin Z, Yang G. New type high-index dielectric nanosensors based on the scattering intensity shift. Nanoscale. 2016;**8**:5996-6007. DOI: 10.1039/C5NR07871G

[24] Yan J, Lin Z, Liu P, Yang G. A design of Si-based nanoplasmonic structure as an antenna and reception amplifier for visible light communication. Journal of Applied Physics. 2014;**116**:154307. DOI: 10.1063/1.4898684

[25] Yan J, Ma C, Liu P, Wang C, Yang G. Generating scattering dark states through the fano interference between excitons and an individual silicon nanogroove. Light: Science & Applications. 2017;**6**:e16197. DOI: 10.1038/lsa.2016.197

[26] Chen H, Nanz S, Abass A, Yan J, Gao T, Choi D-Y, et al. Enhanced directional emission from monolayer WSe_2 integrated onto a multiresonant silicon-based photonic structure. ACS Photonics. 2017;**4**:3031-3038. DOI: 10.1021/acsphotonics.7b00550

[27] Cihan AF, Curto AG, Raza S, Kik PG, Brongersma ML. Silicon Mie resonators for highly directional light emission from monolayer MoS_2. Nature Photonics. 2018;**12**:284-290. DOI: 10.1038/s41566-018-0155-y

[28] Léonard F, Talin AA, Swartzentruber B, Picraux S. Diameter-dependent electronic transport properties of Au-catalyst/Ge-nanowire Schottky diodes. Physical Review Letters. 2009;**102**:106805. DOI: 10.1103/PhysRevLett.102.106805

[29] Sze SM, Ng KK. Physics of Semiconductor Devices. USA: John Wiley & Sons; 2006

[30] Hauser J, Littlejohn M. Approximations for accumulation and inversion space-charge layers in semiconductors. Solid State Electronics.

1968;**11**:667-674. DOI: 10.1016/0038-1101(68)90069-5

[31] Qian F, Kim DM, Kawamoto GH. Inversion/accumulation-mode polysilicon thin-film transistors: Characterization and unified modeling. IEEE Transactions on Electron Devices. 1988;**35**:1501-1509. DOI: 10.1109/16.2583

[32] Lewi T, Iyer PP, Butakov NA, Mikhailovsky AA, Schuller JA. Widely tunable infrared antennas using free carrier refraction. Nano Letters. 2015;**15**: 8188-8193. DOI: 10.1021/acs.nanolett.5b03679

[33] Sokolowski-Tinten K, von der Linde D. Generation of dense electron-hole plasmas in silicon. Physical Review B. 2000;**61**:2643. DOI: 10.1103/PhysRevB.61.2643

[34] Mak KF, He K, Lee C, Lee GH, Hone J, Heinz TF, et al. Tightly bound trions in monolayer MoS_2. Nature Materials. 2013;**12**:207-211. DOI: 10.1038/nmat3505

[35] Newaz A, Prasai D, Ziegler J, Caudel D, Robinson S, Haglund R Jr, et al. Electrical control of optical properties of monolayer MoS_2. Solid State Communications. 2013;**155**:49-52. DOI: 10.1016/j.ssc.2012.11.010

[36] Pei J, Yang J, Xu R, Zeng YH, Myint YW, Zhang S, et al. Exciton and trion dynamics in bilayer MoS_2. Small. 2015;**11**:6384-6390. DOI: 10.1002/smll.201501949

[37] Doerk GS, Carraro C, Maboudian R. Temperature dependence of Raman spectra for individual silicon nanowires. Physical Review B. 2009;**80**:073306. DOI: 10.1103/PhysRevB.80.073306

[38] Hoyland J, Sands D. Temperature dependent refractive index of amorphous silicon determined by time-resolved reflectivity during low fluence excimer laser heating. Journal of Applied Physics. 2006;**99**:063516. DOI: 10.1063/1.2186378

[39] Xu Q, Schmidt B, Pradhan S, Lipson M. Micrometre-scale silicon electro-optic modulator. Nature. 2005; **435**:325-327. DOI: 10.1038/nature03569

[40] Bao W, Myhro K, Zhao Z, Chen Z, Jang W, Jing L, et al. In situ observation of electrostatic and thermal manipulation of suspended graphene membranes. Nano Letters. 2012;**12**: 5470-5474. DOI: 10.1021/nl301836q

[41] Desai SB, Seol G, Kang JS, Fang H, Battaglia C, Kapadia R, et al. Strain-induced indirect to direct bandgap transition in multilayer WSe_2. Nano Letters. 2014;**14**:4592-4597. DOI: 10.1021/nl501638a

[42] Hui YY, Liu X, Jie W, Chan NY, Hao J, Hsu Y-T, et al. Exceptional tunability of band energy in a compressively strained trilayer MoS_2 sheet. ACS Nano. 2013;**7**:7126-7131. DOI: 10.1021/nn4024834

[43] Dhakal KP, Roy S, Jang H, Chen X, Yun WS, Kim H, et al. Local strain induced band gap modulation and photoluminescence enhancement of multilayer transition metal dichalcogenides. Chemistry of Materials. 2017;**29**:5124-5133. DOI: 10.1021/acs.chemmater.7b00453

[44] Roldán R, Castellanos-Gomez A, Cappelluti E, Guinea F. Strain engineering in semiconducting two-dimensional crystals. Journal of Physics. Condensed Matter. 2015;**27**:313201. DOI: 10.1088/0953-8984/27/31/313201